Stochastic Approach for the Prediction of PSD in Nonisothermal Antisolvent Crystallization Processes

Giuseppe Cogoni, Stefania Tronci, Giuseppe Mistretta, and Roberto Baratti
Dipartimento di Ingegneria Meccanica, Chimica e dei Materiali, Università degli Studi di Cagliari, Piazza D'Armi, I-09123, Cagliari, Italy

Jose A. Romagnoli
Dept. of Chemical Engineering, Louisiana State University, South Stadium Road, Baton Rouge, LA 70803

DOI 10.1002/aic.14089
Published online March 26, 2013 in Wiley Online Library (wileyonlinelibrary.com)

A stochastic formulation for the description of cooling-antisolvent mediated crystal growth processes based on the Fokker-Planck equation is discussed. Previous results are further extended to include not only the additional degree of freedom (temperature) in the approach, but also to formulate the model parameters dependencies with the input manipulated variables (antisolvent flow rate and temperature) toward a global model to be used within all possible operating regimes. The obtained global models are used to define, for the first time, an operating map of the crystallization process, where asymptotic isomean and isovariance curves are reported in an antisolvent flow-rate-temperature plane. Input multiplicities are identified and validated both numerically and experimentally for the NaCl-water-ethanol nonisothermal antisolvent crystallization system. © 2013 American Institute of Chemical Engineers *AIChE J*, 59: 2843–2851, 2013

Keywords: antisolvent crystallization, nonisothermal crystallization, global model, Fokker-Planck equation

Introduction

Antisolvent aided crystallization is an advantageous separation technique when the solute is highly soluble or heat sensitive. The driving force in crystal formation is the supersaturation that establishes the thermodynamic equilibrium for the solid–liquid separation. The main technologies used to obtain the super-saturation are cooling of the solution and antisolvent addition, and a proper combination of them could improve the quality of the product, as recently demonstrated for few systems.[1,2] The organic systems, paracetamol and acetyl-salicylic acid, used in the aforementioned two articles have solubilities that change significantly with temperature, therefore, to incorporate cooling with antisolvent crystallization can significantly increase crystallization yield. It has also been shown recently[3] that even for systems with solubility weakly dependent on temperature; it is possible to impart significantly improved control over both the distribution mean size and coefficient of variation by manipulating temperature together with antisolvent feed rate. This strategy would allow us to add a second degree of freedom (cooling) to be used to control the crystallization process.

The control of the crystal size and the crystal size distribution is an important and challenging problem and several factors can affect the size and the widening of the size distribution. The development of effective mathematical models describing the crystal growth dynamics is, therefore, a crucial issue toward finding the optimal process performance and to control the crystal size and distribution. Antisolvent crystallization has been modeled for many systems using the traditional population balance modeling approach.[4–9] As an alternative, it was recently shown[10,11] that it is possible to describe a crystallization process by means of a stochastic approach, which allows the obtainment of the crystal size distribution (CSD) evolution with respect to time using the Fokker-Planck equation. Furthermore, this type of representation leads to simpler models and allow for the analytical solution to describe the CSD over time in antisolvent crystallization operations in the case of linear growth term[11] and in asymptotic CSD for nonlinear growth term.[12] However, the Fokker-Planck-based model does not have an explicit dependency of the control input (i.e., antisolvent flow rate), and/or the temperature, although these variables do affect the process parameters. In order to use the model over the whole operating range, linear piece-wise interpolation approaches have been so far exploited[10–12] as a function of a single input (antisolvent flow rate). Even though effective results were obtained, the use of linear interpolation can be difficult to use when a continuous input-output relationship is required, as in case of model-based control algorithms. Furthermore, when temperature dependency is incorporated, a typical experimental campaign with three temperature levels and three antisolvent flow rate values requires the implicit estimation of 27 different parameter values.

In order to use the model over the whole operational range proper relationships between the parameters of the model and the two process variables, namely antisolvent flow rate and temperature, has to be developed. Consequently, in this

Correspondence concerning this article should be addressed to R. Baratti roberto.baratti@dimcm.unica.it.

work, we further extend previous results, in the Fokker-Planck modeling approach, to include not only the additional degree of freedom (temperature) in the formulation, but also to formulate the model parameters dependencies with the input manipulated variables (antisolvent flow rate and temperature) toward a global model to be used within all possible operating regimes. In the proposed formulation, the input-parameter models should have simple linear or quadratic dependences, while the cross term dependence on temperature and antisolvent flow rate should be avoided, leading to a significant reduction with respect to the piece-wise linearization approach. The Akaike information criteria (AIC) measure has been used for the selection of the best input-output model.

Furthermore, as an additional novelty, the obtained global models are used to define an operating map of the crystallization process, where asymptotic isomean and isovariance curves are reported in an antisolvent flow-rate-temperature plane. In our formulation, the asymptotic CSD for the map construction can be analytically obtained using the reported analytical expressions for the asymptotic solution arising from the Fokker-Planck representation.[12] This procedure leads to find out that the same distribution, in terms of the first two moments, can be obtained at different operating conditions, thus, implying an input multiplicity of the system, which is consistent with the opposite effects that antisolvent flow rate and temperature have on the crystallization process. The input multiplicity obtained by solving the model have also been validated experimentally, by conducting additional set of experiments, thus, confirming the behavior predicted by the model and the effectiveness of the operational map.

Results are provided through investigations in the nonisothermal antisolvent crystallization of sodium chloride (NaCl), the solubility of which is practically independent of temperature. An antisolvent feed-rate-dependent crystallization model is developed and validated for the nonisothermal operation of NaCl-water-ethanol antisolvent crystallization system.

The article is organized as follows. The section *Experimental Work* fully describes the setup of the experimental rig and the procedure. The *Stochastic Modeling Approach* section is a short description of the stochastic approach for crystal size distribution, followed by the parameter estimation problem formulation. In the *Stochastic Global Model* section, the formulation of alternative global models is described and the proposed dependencies of the model parameters with the input manipulated variables are introduced. The section *Operational Maps* reported asymptotic isomean and isovariance curves, in an antisolvent flow-rate-temperature plane, and finally *Conclusions*.

Experimental Work

The experiments were performed in a bench-scale crystallizer, where only purified water, reagent grade sodium chloride (99.5%) and ethanol, 190 proof, were used. The experimental setup and procedure are described as follows.

Experimental setup

The experimental rig is comprised of a one liter jacketed reactor connected to a Thermo Scientific® cooling/heating bath circulator that provides to keep constant the temperature inside the reactor by an embedded PID controller and a thermocouple wired inside the reactor. The antisolvent is added using a Masterflex® peristaltic pump calibrated for each experiment. The crystal size distribution is determined from the images of the samples taken from the reactor using a digital camera mounted in a stereomicroscope and then processed by means of sizing computer software (Amscope®).

Experimental procedure

At the startup condition, the crystallizer is loaded with an aqueous solution of NaCl made up of 34 *g* of NaCl dissolved in 100 g of water. The temperature is kept constant throughout the run, using three different values for the temperature, respectively, 10°C (hereafter referred to as low temperature: LT), 20°C (medium temperature: MT), and 30°C (high temperature: HT). The ethanol was added to the aqueous NaCl solution using a calibrated peristaltic pump. Three different antisolvent flow rates were implemented: $q = 0.7$ mL/min (hereafter referred as low feed rate: LFR), $q = 1.5$ mL/min (medium feed rate: MFR) and $q = 3.0$ mL/min (high-feed rate: HFR). Thus, a full factorial experimental design of nine experiments was performed. Along the operation, 8 mL samples were taken in an infrequent fashion. Samples were then vacuum-filtered over filter paper and then dried in an oven, at least for 24 h, with a constant temperature of 50°C for further visual inspection.[10]

Crystal size measurement

Crystal size measurement has been accomplished by means of a light microscopy. A stereo light microscope (Wild-Heerbrugg, Switzerland) was used and connected to a digital camera (Amscope Model MD500, USA). Several images were taken with the camera for each sample and analyzed using the AmScope software (iScope, USA). The software allows for the measurement of the length or area of particular crystals in units of pixels. Using a supplied calibration slide, these lengths and areas can be converted to a micron length-scale. The number of crystals measured varied for each sample and was fixed by a stabilization criterion of $\pm 2.5\%$ of the mean.

Stochastic Modeling Approach

The crystallization process has been modeled using the approaches proposed previously,[10,13,14] where the growth of crystal size L is assumed to be governed by a deterministic and a stochastic term

$$\frac{dL}{dt} = Lg(L;\theta) + L\eta(t) \tag{1}$$

In Eq. 1 $g(L;\theta)$ represents the deterministic contribution to the growth rate of L, θ is the vector parameter defined in the model, $L\eta(t)$ is the a random component linearly depending on crystal size and $\eta(t)$ is the Langevin force. It is further assumed that

$$\begin{aligned} E[\eta(t)] &= 0 \\ E[\eta(t)\eta(t')] &= 2\Lambda\delta(t-t') \end{aligned} \tag{2}$$

where Λ is the intensity of the Langevin force, which has been assumed as constant and equal to $\sqrt{D}$, with D being the diffusivity parameter. Dividing both terms of Eq.1 by L, the Langevin equation becomes

Table 1. Expressions used to Describe the Growth Process, where i = 1, 2, $\theta_1 = (r_1, K_1)$ and $\theta_2 = (r_2, K_2)$

	Model 1	Model 2
$g(y;\theta_i)$	$r_1 y\left(1-\frac{y}{K_1}\right)$	$r_2\left(1-\frac{y}{K_2}\right)$

$$\frac{dy}{dt} = g(y;\theta) + \eta(t) \tag{3}$$

where y is defined as $y = \ln L$.

Regarding the selection of the deterministic model $g(y;\theta)$, one should adopt a structure as simple as possible, while preserving the main features expected by a growth process. In this work, a logistic equation[10] and a Gompertz model[11] are assumed for describing the growth term (Table 1), which hereafter will be generally indicated with $g(y;\theta_i)$ and $i = 1$ will denote the logistic model, Model 1, whereas $i = 2$ the Gompertz model, Model 2.

The probability density function (PDF) related to the y random variable can then be described by the following Fokker-Planck equation[10]

$$\frac{\partial\psi(y,t)}{\partial t} = D\frac{\partial^2\psi(y,t)}{\partial y^2} - \frac{\partial}{\partial y}[g(y,t;\theta_i)\psi(y,t)] \quad t \geq 0, y \in \Re \tag{4}$$

where $g(y;\theta_i)$ can assume one of the two expressions reported in Table 1, and the initial condition for $t = t_0$ is assumed as a normal distribution[11]

$$\psi(y,t_0) = \frac{1}{\sigma_0\sqrt{2\pi}}\exp\left[-\frac{(y-\mu_0)^2}{2\sigma_0^2}\right] \tag{5}$$

where μ_0 and σ_0 are, respectively, the initial mean size of crystals (logarithmic scale) and the standard deviation at $t = t_0$. It is worth noticing that the FPE could be considered as an alternative way to develop a population balance,[15] taking into account the natural fluctuations present in the population in any system, and allowing describing, in a compact form, the population dynamics.

When the Model 1 is considered the analytical solution of Eq. 4 is not available; therefore, the crystal size distribution (CSD) is obtained by numerical integration. Conversely, when the growth term is described by the linear expression, the PDF will preserve its Gaussian shape at any time[12], thus, the distribution is described by its first two moments, the mean μ, and the variance σ^2

$$\psi(y,t) = N\left(\mu(t),\sigma^2(t)\right) \tag{6}$$

The first moment then follows the deterministic Gompertz equation (in logarithmic scale), and, therefore, the analytical solution is possible and given by[11]

$$\mu(t) = K_2\left\{1-\left(1-\frac{\mu_0}{K_2}\right)\exp\left[-\frac{r_2}{K_2}(t-t_0)\right]\right\} \tag{7}$$

The dynamics of the second moment is described by the following differential equation[16]

$$\frac{d\sigma^2(t)}{dt} = 2D_2 - 2A\sigma^2(t) \tag{8}$$

where A is the coefficient of the state variable of the system, equal to $-\frac{r_2}{K_2}$, and σ^2 is the variance. Thus, the analytical solution for the time evolution of the variance $\sigma^2(t)$ is given by

$$\sigma^2(t) = \sigma_0^2\exp\left[-2\frac{r_2}{K_2}(t-t_0)\right] + \frac{D_2K_2}{r_2}\left(1-\exp\left[-2\frac{r_2}{K_2}(t-t_0)\right]\right) \tag{9}$$

The three parameters (r_i, K_i, D_i), with $i = 1, 2$, of the considered models depend on the crystallizer conditions, which in the case of nonisothermal antisolvent crystallization are the antisolvent flow rate and temperature.

It is worth noticing that the first two moments of the distribution $\Psi(y,t)$ for Model 1 and 2 can then be evaluated, in the linear scale, as

$$\mu_L(t) = \int_0^\infty L\psi(L,t)dL = \exp\left[\mu_y(t) + \frac{\sigma_y^2(t)}{2}\right] \tag{10}$$

$$\sigma_L^2(t) = \int_0^\infty (L-\mu_L)^2\psi(L,t)dL = \exp\left[2\mu_y(t)+\sigma_y^2(t)\right]\left(\exp\left[\sigma_y^2(t)\right]-1\right) \tag{11}$$

Parameter Estimation

Parameters estimation for the FPE describing the crystal growth for both linear and nonlinear models (Table 1) has been first carried out separately for every operating condition. In particular, experimental data obtained by the full factorial experimental design of nine runs have been used (see Experimental Work section).

The θ_i vector of parameters (where $i = 1, 2$) have been obtained by means of the maximum likelihood estimation approach. In particular, the parameters are inferred by maximizing the log-likelihood function considering all the n_t experimental data collected at different operating conditions:

$$ln L(\theta_i|y_m) = ln\prod_{m=1}^{n_t}\psi\left(y_m\left(t_{j,k}\right),\theta_i\right) = \sum_{k=1}^{n_e}\sum_{j=1}^{n_k}\sum_{l=1}^{n_{j,k}} ln\,\psi\left(y_{l,k}\left(t_{j,k}\right)\right)$$
$$n_t = \sum_{k=1}^{n_e}\sum_{j=1}^{n_k} n_{j,k} \tag{12}$$

where y_m is the value in logarithmic scale of the m-th experimental observation for the crystal size ($m = 1, \ldots, n_t$), n_e is the number of experimental runs carried out varying input parameters, n_k is the number of sampling time, $n_{j,k}$ is the number of crystal size measurements collected at time $t_{j,k}$. It is worth noting that when Model 1 is assumed, the parameter estimation is performed using the PDF $\Psi(y,t)$ obtained by numerical integration of (4). In the linear model case, $\Psi(y,t)$ is a Gaussian distribution with mean and variance calculated by means of Eqs. 7 and 9.

Table 2 reports the point estimations for the model parameters for both Model 1 and Model 2. The following behavior can be appreciated, which sounds from a physical point of view (1) r_i increases with antisolvent flow rate and decreases with temperature, (2) K_i decreases with antisolvent flow rate and increases with temperature and (3) D_i increases with antisolvent flow rate and decreases with temperature.

Table 2. Model Parameters Calculated at Different Operating Conditions for Logistic (Model 1) and Linear (Model 2) Crystal Growth Law

	Model 1			Model 2		
r	**10°C**	**20°C**	**30°C**	**10°C**	**20°C**	**30°C**
0.7 ml/min	1.0646	1.5700	0.7312	4.278	6.938	2.992
1.5 ml/min	1.9343	1.4029	1.1030	8.837	6.117	5.294
3.0 ml/min	3.2860	3.4428	1.9420	13.757	14.122	8.629
K	**10°C**	**20°C**	**30°C**	**10°C**	**20°C**	**30°C**
0.7 ml/min	4.9303	4.9501	5.0713	4.899	4.897	5.046
1.5 ml/min	4.8583	4.9298	5.0489	4.816	4.900	5.011
3.0 ml/min	4.7095	4.7656	4.8659	4.661	4.725	4.835
D	**10°C**	**20°C**	**30°C**	**10°C**	**20°C**	**30°C**
0.7 ml/min	0.1957	0.3992	0.1270	0.181	0.399	0.112
1.5 ml/min	0.3732	0.2163	0.1713	0.371	0.208	0.179
3.0 ml/min	0.7186	0.6735	0.2912	0.699	0.626	0.281

In fact, increasing antisolvent flow rate leads to higher nucleation rates (r increases), but reduces the average asymptotic crystal size (K decreases). Temperature has an opposite effect as already discussed[3] in the nonisothermal antisolvent crystallization of sodium chloride (NaCl). Higher values of temperature, decreases r and reduces the driven force for nucleation and favors crystal growth (K increases). The operating conditions that favor nucleation determine a higher dispersion of the PSD, and this aspect has been correctly reconstructed by the behavior of coefficient D.

Stochastic Global Model

As discussed previously in the Introduction, the proposed crystallization models based on FPE do not have an explicit dependency from operating conditions. In order to use the model over the whole operating range, linear piece-wise interpolation approaches have been so far exploited[10–12] for the isothermal operation (single input manipulated variable).

Table 3. Values of the Model Parameters Describing the Dependence of (r, K, D) on Antisolvent Flow Rate and Temperature

Coefficient	Model 1	Model 2
$\gamma_{i,0r}$	0.5264	5.7639
$\gamma_{i,1r}$	0.5983	2.8342
$\gamma_{i,2r}$	$-6.4588\ 10^{-4}$	-0.1584
$\gamma_{i,0K}$	4.9176	4.8593
$\gamma_{i,1K}$	-0.0238	-0.0244
$\gamma_{i,2K}$	$1.7139\ 10^{-4}$	$2.0\ 10^{-4}$
$\gamma_{i,0D}$	0.2134	0.3864
$\gamma_{i,1D}$	0.0277	0.0287
$\gamma_{i,2D}$	-0.0019	-0.0094

However, for the nonisothermal condition, a typical experimental campaign with three temperature levels and three antisolvent flow rate values requires the implicit estimation of 27 different parameter values if piece-wise linear interpolation is used. Furthermore, although effective results were obtained, the use of linear interpolation can be difficult to use when a continuous input-output relationship is required, as in case of model-based control algorithms.

In this work, the FPE is generalized in order to take into account an explicit dependence of the stochastic model parameters on input variables $m = (q, T)$

$$\frac{\partial \psi(y,t)}{\partial t} = D_i(m)\frac{\partial^2 \psi(y,t)}{\partial y^2} - \frac{\partial}{\partial y}\psi(y,t)g(y;\theta_i(m))\ i=1,2 \quad (13)$$

The main goal is to find simple and parsimonious models that can describe the variation of the vector parameter θ_i with q and T, coherently with the behavior obtained for the point estimation reported in the previous paragraph. From the inspection of the results in Table 2 and considering the

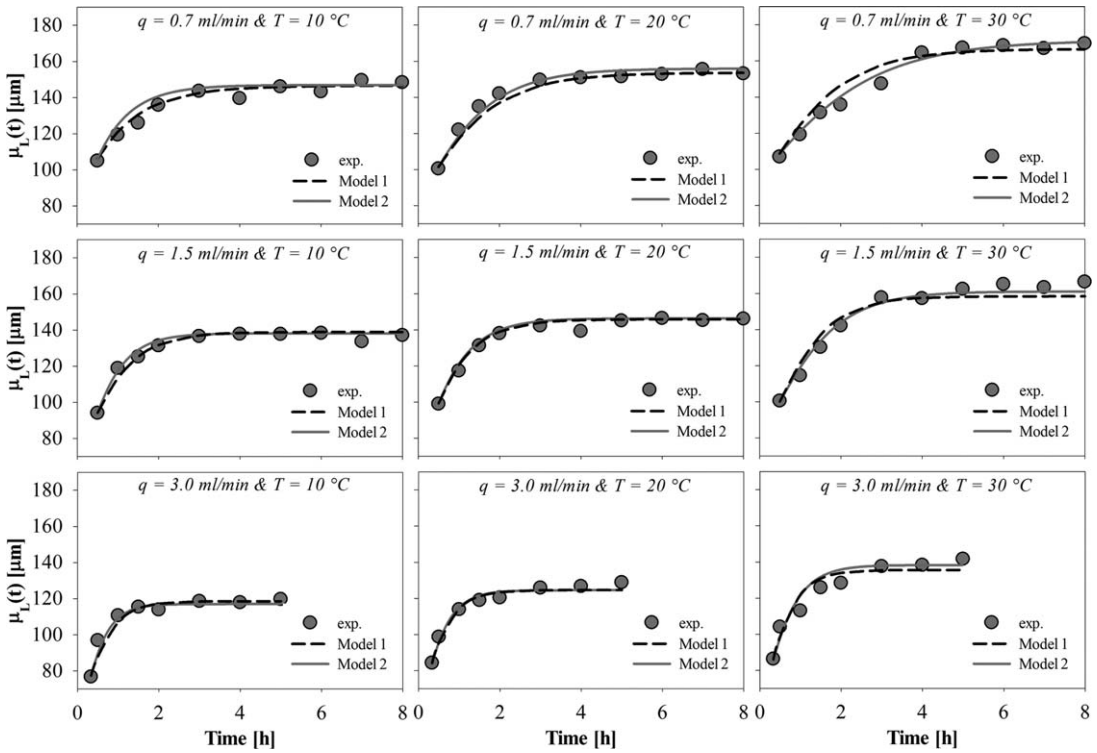

Figure 1. Mean size evolution of the nine experimental runs considered: (dash line) Model 1; (solid line) Model 2; (circle) experimental values.

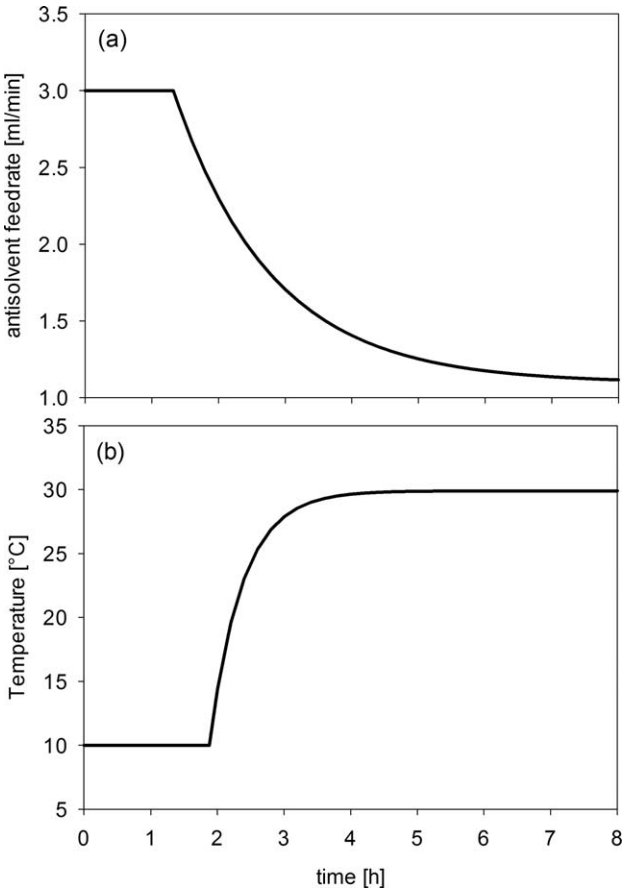

Figure 2. Antisolvent flow rate (a) and temperature, and (b) trajectory used for the validation run.

experimental error, it is possible to hypothesize that the model parameters can have a nonlinear or weak nonlinear dependence on inputs. From the aforementioned considerations, the proposed input-parameter models are required satisfy the following conditions: (1) simple linear or quadratic dependences have been preferred to describe the input-parameter relationships, and (2) the cross term dependence on T and q should be avoided. Despite these simplifications, each parameter may depend on several combinations of T and q, thus, leading to a number of alternative models. In this work, the following general expression for the parameter dependencies have been considered

$$\begin{aligned} r_{\mathrm{i}}(q,T) &= \gamma_{\mathrm{i},0r} + \gamma_{i,1r} q^{\mathrm{a}_r} + \gamma_{i,2r} T^{\mathrm{b}_r} \\ K_{\mathrm{i}}(q,T) &= \gamma_{\mathrm{i},0K} + \gamma_{i,1K} q^{\mathrm{a}_K} + \gamma_{i,2K} T^{\mathrm{b}_K} \; i = 1,2 \\ D_{\mathrm{i}}(q,T) &= \gamma_{\mathrm{i},0D} + \gamma_{i,1D} q^{\mathrm{a}_D} + \gamma_{i,2D} T^{\mathrm{b}_D} \end{aligned} \tag{14}$$

where a_v and b_v can be equal to 1 or 2 for $v = r, K, D$. In this way, the functions obtained to correlate the vectors θ_{i} with the manipulated variables q and T have nine parameters, leading to a significant reduction with respect to the piece-wise linearization approach. The Γ vector of $\gamma_{\mathrm{i,u}v}$ parameters (where $\mathrm{u} = 0, 1, 2$ and $v = r, K, D$) have been again obtained by means of the a maximum likelihood estimation approach (c.f., Eq. 12).

The detection of the most suited model among the possible alternatives that depends on the functionality of q and T has been performed coupling a quantitative and qualitative analysis of the results. The former issue has been assessed exploiting the Akaike information criterion (AIC) measure, which considers the maximum likelihood fitting of each model and each set of exponents. The qualitative evaluation has been based on the ability of the model to represent the multiplicity of the asymptotic conditions, according to the behavior of K parameter. The models satisfying the considered criteria for both nonlinear (Model 1) and linear (Model 2) crystal growth expressions are given by

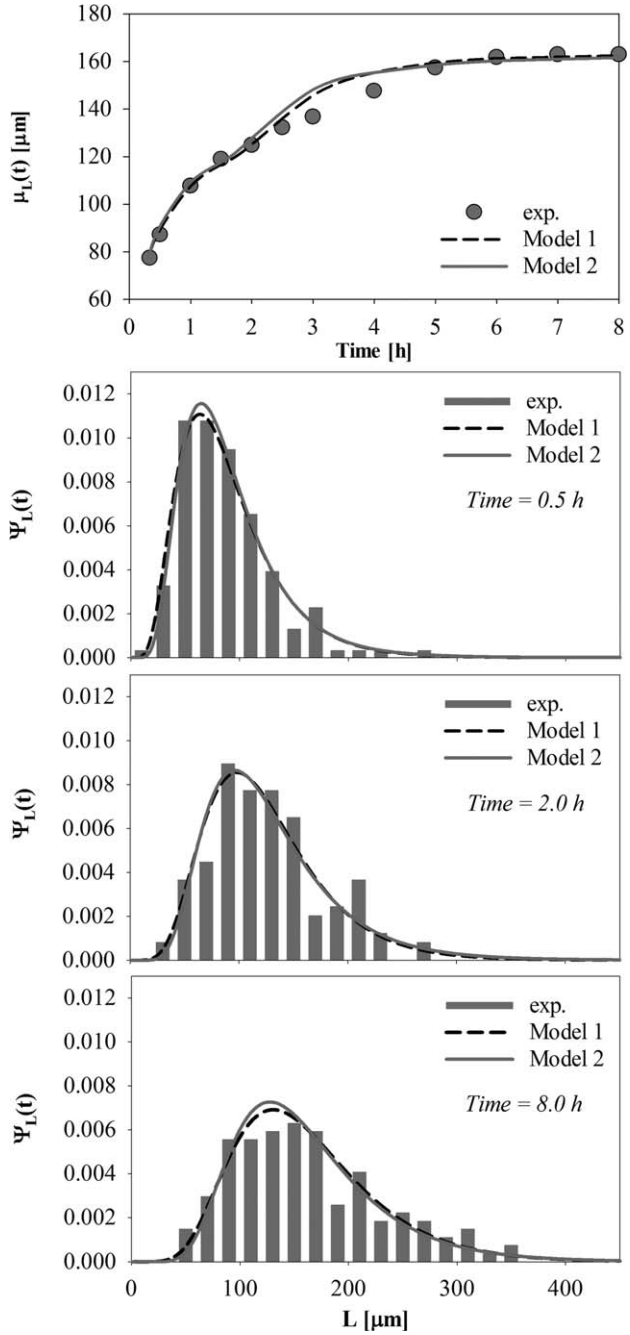

Figure 3. Validation results obtained in terms of mean sizes (top diagram) and CSDs (plots at the bottom): (dash line) Model 1; (solid line) Model 2; (circle/bar) experimental data.

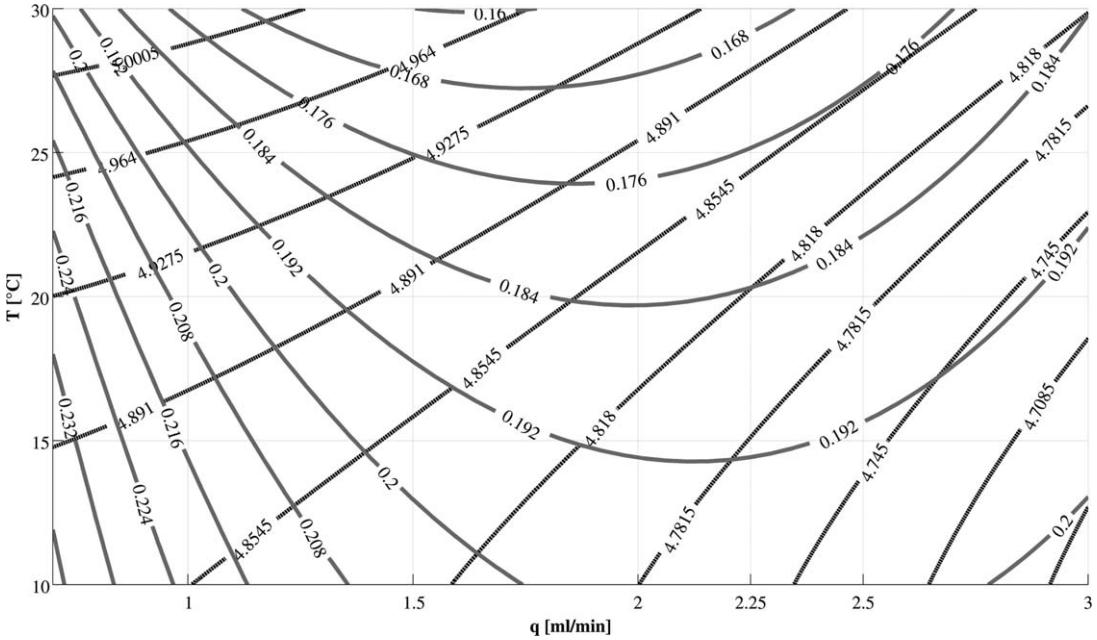

Figure 4. Isomeans/isovariances map, logarithmic scale, reported in function of *T* and *q*, for the Model 2: (dash line) mean; (solid line) variance.

$$
\begin{aligned}
r_i(q,T) &= \gamma_{i,0r} + \gamma_{i,1r} q + \gamma_{i,2r} T \\
K_i(q,T) &= \gamma_{i,0K} + \gamma_{i,1K} q^2 + \gamma_{i,2K} T^2 \quad i = 1,2 \\
D_i(q,T) &= \gamma_{i,0D} + \gamma_{i,1D} q^2 + \gamma_{i,2D} T
\end{aligned}
\tag{15}
$$

The coefficients of expressions (15) are reported in Table 3, where it is possible to verify that the behavior shown by the parameter obtained performing the estimation for every operating condition are maintained by the proposed models. For example, the negative sign of $\gamma_{i,1K}$ is explainable with the fact that increasing antisolvent flow rate makes the asymptotic crystal size to decrease (high q values favor nucleation with respect to crystal growth). The same unfavorable effect of temperature on crystal growth rate (r_i), and dispersion (D_i), is correctly described being $\gamma_{i,2r}$ and $\gamma_{i,2D}$ negative.

The capability of the proposed global model to properly describe the crystallization system is shown in Figure 1, which reports the experimental mean crystal size behavior collected during the nine runs described on the Experimental Work section, and the value calculated by solving FPE (13): numerically when using Model 1 (dash line) and analytically for Model 2 (solid line). The match between calculated $\mu_L(t)$ and experimental values is excellent for both models, indicating that Eqs. 15 correctly approximate the input-parameter relationships.

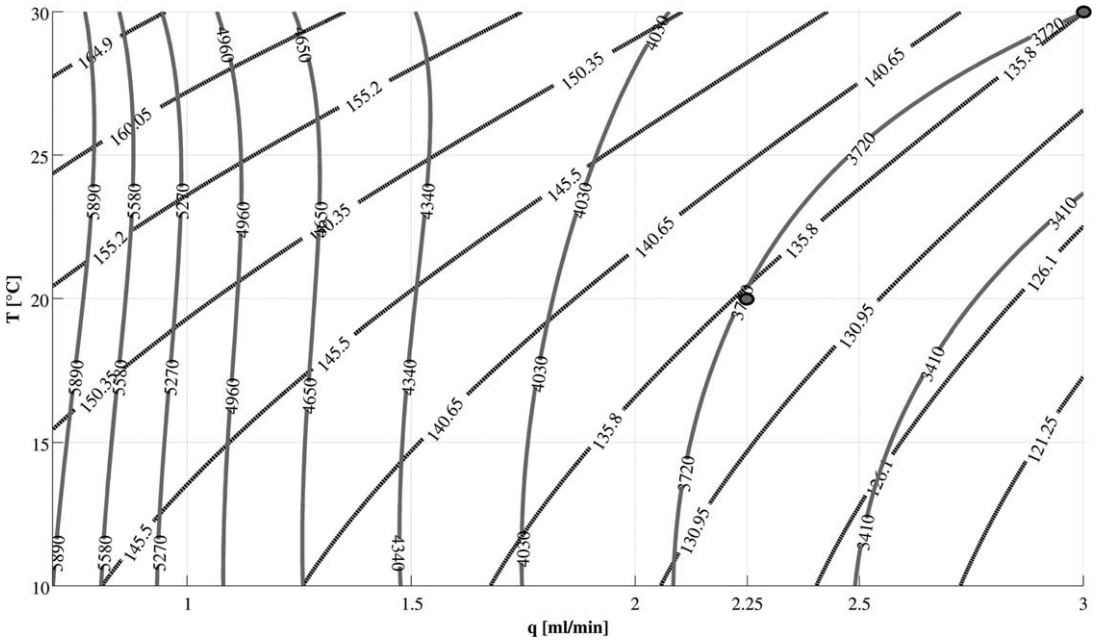

Figure 5. Isomeans/isovariances map, linear scale, using Model 2: (dash line) mean; (solid line) variance.

The circle is indicating the validation run.

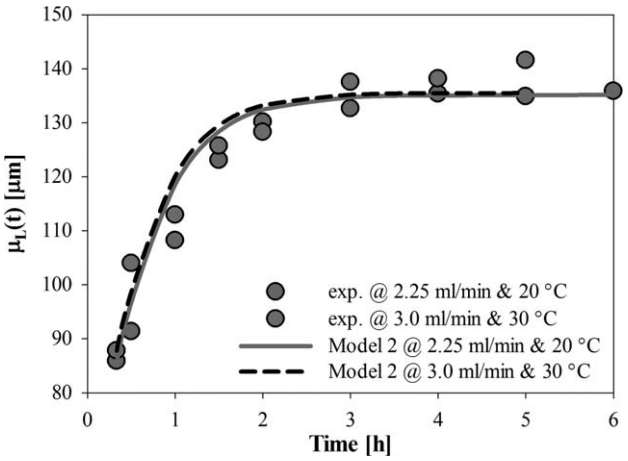

Figure 6. Comparison between computed (Model 2) and the experimental values in the multiplicity point: (solid line/red circle) run at 2.25 mL/min and 20°C; (dash line/gray circle) run at 3.0 mL/min and 30°C.

The obtained global models have been also validated considering the antisolvent flow rate and temperature trajectory reported in Figure 2. The results in terms of mean crystal size evolution are reported in the top of Figure 3, where the comparison with the experimental data indicates that both Model 1 (dashed line) and Model 2 (solid line) again have excellent prediction capabilities, during the nonisothermal operation of the system. The obtained models are also excellent predictors of the crystal size distribution, as shown again in Figure 3, where the time evolution of the experimental and calculated CSD is reported at different sampling time.

It is worth noticing that the results obtained with linear and nonlinear growth rate are very close both considering the mean crystal size behavior and the CSD. This implies that assumption of linearity allows to a very good description of the considered system and could offer a more practical tool with respect to the nonlinear model, when model-based optimal controller wants to be developed.

Operational Map

The obtained global models can be used to define the operating conditions of the crystallization process, leading to the desired mean and variance of the crystal size distribution. In order to have a functioning tool for designing the proper crystallization runs, a map can be constructed where asymptotic isomean and isovariance curves are reported in an antisolvent flow-rate-temperature plane. In this case, the asymptotic CSD for the map construction can be analytically obtained also for Model 1, using the approach reported in Tronci et al.[12] which leads to the following expression for the stationary solution of Eq. 13

$$\psi_1(y)=N_{S1}\exp\left[\int_0^y g(\zeta,\theta_1)\mathrm{d}\zeta\right] \qquad N_{S1}=\frac{1}{\int_{-\infty}^{+\infty}\exp\left[\int_0^y g(\zeta;\theta_1)\mathrm{d}\zeta\right]\mathrm{d}y} \tag{16}$$

In particular, the stationary solution for Model 1 is

$$\psi_1(y)=N_{S1}\exp\left[\frac{r_1}{D_1}\left(\frac{y^2}{2}-\frac{y^3}{3K_1}\right)\right] \qquad N_{S1}=\frac{1}{\int_{-\infty}^{+\infty}\exp\left[\frac{r_1}{D_1}\left(\frac{y^2}{2}-\frac{y^3}{3K_1}\right)\right]\mathrm{d}y} \tag{17}$$

The stationary CSD for Model 2 is easily obtained from a Gaussian distribution with mean equal to K_2 and variance equal to K_2D_2/r_2 (see Eqs. 7 and 9)

$$\psi_2(y)=\frac{1}{\sqrt{2\pi K_2D_2/r_2}}\exp\left[-\frac{1}{2}\frac{(x-K_2)^2}{K_2D_2/r_2}\right] \tag{18}$$

For sake of brevity, only the map for Model 2 (linear growth rate) has been reported at different operating

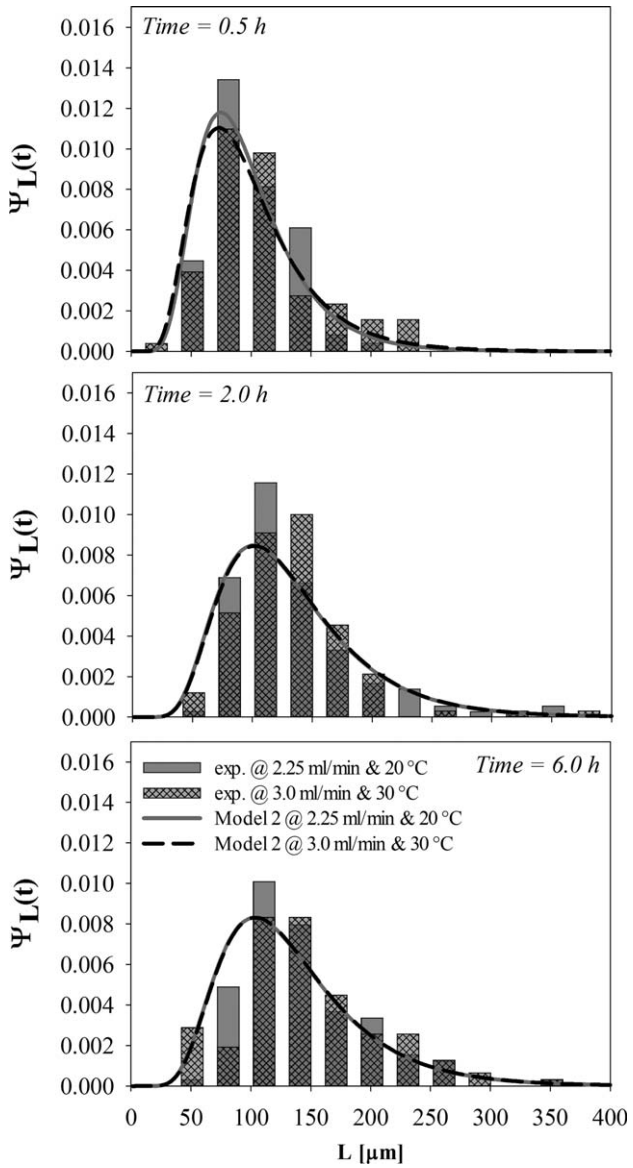

Figure 7. CSDs at the multiplicity points at different time steps: (solid line/red bar) run at 2.25 mL/min and 20°C; (dash line/gray bar) run at 3.0 mL/min and 30°C.

conditions. As demonstrated in the previous paragraph, the behavior of the two models are almost overlapping, therefore, the results reported in Figure 4 are representative of both linear and nonlinear case.

By inspection of Figure 4 it is interesting to note that isovariance curves may intersect isomean curves in two points, therefore, the same distribution in terms of the first two moments can be obtained at different operating conditions. Considering Figure 4, a CSD with mean crystal size (logarithmic scale) equal to 4.818 and variance equal to 0.184 is attained at (q, T) = (2.25, ~21.0) and (q, T) = (3.0, 30). This result implies some kind of input multiplicity of the system, which is coherent with the opposite effects that antisolvent flow rate and temperature have on the crystallization process: high asymptotic crystal size can be reached with low q and high T, but the same result can be obtained increasing q and, at the same time, decreasing T. Figure 4 has been also represented in linear scale in Figure 5, accordingly to the nonlinear transformation Eqs. 10 and 11.

To corroborate these findings and confirm the goodness of the selected model, an additional experiment was conducted at q = 2.25 mL/min and T = 20°C (indicated with a circle in Figure 5). The multiplicity of the considered crystallization system with respect to inputs can now be verified by considering the time evolution of the experimental mean crystal size at (q, T) = (3.0 mL/min, 30°C) and (q, T) = (2.25 mL/min, 20°C), and compared with the results predicted by Model 2 (see Figure 6).

As can be seen in Figure 6, each mean size profile takes a slightly different path to reach the same final value (within the tolerance error associated with the crystal size measurement). At the beginning of the process, higher temperature and antisolvent flow rate speed up the crystallization process, therefore, the mean crystal size is higher with respect to the values obtained at lower q and T. This behavior is also represented by the models, which have different initial conditions. As time elapses, the values predicted by the two models at different operating conditions converge, as well as the experimental mean crystals size values, as expected considering the isomean and isovariance map.

The input multiplicity can be also verified by looking at the experimental and calculated CSD at different sampling time (Figure 7). Again, there is a slight mismatch at the beginning sampling times, but the asymptotic values predicted by the map are confirmed at the end of batch (time-= 5–6 h), where there is a significant overlapping between the histograms of the crystal size obtained at (q, T) = (2.25 mL/min, 20°C) and at (q, T) = (3.0 mL/min, 30°C). There is also a perfect match between the two models, evidencing that linear assumption does not worsen the description of the considered system. This fact is important because a linear convective term in the FPE allows solving analytically the Fokker-Planck equation, giving an effective tool for online optimization and model-based control of the process.

Conclusions

The crystallization aided antisolvent process has been here described by means of the Fokker-Planck approach, including the dependencies on the manipulated inputs, which are the antisolvent flow rate and temperature, and considering both nonlinear and linear crystal growth rate. The model parameters, which comprises the deterministic growth rate constants and the diffusivity (related to the stochastic component of the model) have been obtained as a function of process inputs guaranteeing simplicity of the global model, while preserving the physical consistency of the results. It has been further demonstrated that excellent results can be obtained both with nonlinear and linear crystal growth model, by the comparison of the predicted crystal size distributions and the experimental ones. This aspect is of great importance, because the presence of a linear term in the partial differential equation describing the time evolution of the CSD allows for the analytical solution, giving an effective tool for developing process optimization and model-based control strategies.

The obtained model has been also used for the construction of operative maps, where the first two moments of the predicted CSD have been plotted with respect to the operating conditions. These results have been represented as isomean/isovariance maps with respect to antisolvent flow rate and temperature. This representation allows finding that the considered system may show input multiplicity, in the understanding that the same CSD, in terms of mean and variance, can be obtained at different input values. The results have been experimentally validated and applied to both nonlinear and linear crystal growth rate.

Acknowledgments

J. Romagnoli kindly acknowledges the financial support by NSF through the Award # 1132324. Regione Sardegna for the support, through the program "Visiting Professor 2011".

Notation

a = generic exponent for the antisolvent feed rate functionality
A = coefficient of the Ricatti equation, h^{-1}
b = generic exponent for the temperature functionality
D = diffusivity or pseudo-diffusivity constant for the FPE
D_i = diffusivity constant for the ith model, with i = 1, 2
$D_i(m)$ = diffusivity constant for the FPE as a function of the vector variables m
g = deterministic model used for the drift term of the FPE
K_i = asymptotic dimension of crystals in logarithmic scale for the ith model, with i = 1,2
$K_i(q,T)$ = asymptotic dimension of crystals in logarithmic scale for the ith model, with i = 1, 2 as a function of q and T
L = characteristic dimension of crystals, μm
m = vector of manipulated variables q and T
n_t = total number of crystal size measurements
N_{S1} = normalization constant for the steady state FPE, for the model 1
q = antisolvent federate, mL/min
r_i = deterministic growth rate for the ith model, with i = 1, 2, h^{-1}
$r_i(q,T)$ = deterministic growth rate for the ith model, with i = 1, 2 as a function of q and T, h^{-1}
t = time variable, h
t' = perturbative time, h
t_0 = initial time for the integration of the FPE, corresponding to the first experimental sample taken, h
T = temperature of the system, °C
y = characteristic dimension of crystals in logarithmic scale (ln L)
y_m = measured characteristic dimension of crystals in logarithmic scale

Greek letters

$\gamma_{i,j,r}$ = function coefficients for the parameter r, for the ith model with i = 1, 2 and j = 0, 1, 2
$\gamma_{i,j,K}$ = function coefficients for the parameter K, for the ith model with i = 1, 2 and j = 0, 1, 2
$\gamma_{i,j,D}$ = function coefficients for the parameter D, for the ith model with i = 1, 2 and j = 0, 1, 2

Γ = vector of parameters $\gamma_{i,j,k}$, with i = 1, 2, j = 0, 1, 2 and k = *r, K, D*
δ = delta of Dirac
η = white noise
θ = vector of parameters
$\theta_i(m)$ = vector of parameters for the *i*th model, with i = 1, 2 as a function of the vector *m*
Λ = white noise noise intensity
μ = mean size of crystals in logarithmic scale
μ_0 = mean size of crystals in logarithmic scale, evaluated at $t = t_0$
$\mu_L(t)$ = time evolution function of the mean size of crystals in linear scale
σ_0 = standard deviation of crystals in logarithmic scale, evaluated at $t = t_0$
σ^2_0 = variance of crystals in logarithmic scale, evaluated at $t = t_0$
σ^2 = variance of crystals in logarithmic scale
$\sigma^2(t)$ = time evolution function of the variance of crystals in logarithmic scale
$\Psi_i(y)$ = dependent variable of the FPE for the *i*th model, with i = 1, 2
$\Psi(y,t)$ = dependent variable of the FPE
$\Psi(y,t_0)$ = dependent variable of the FPE evaluated at $t = t_0$

Literature Cited

1. Nagy ZK, Fujiwara M, Braatz RD. Modelling and control of combined cooling and antisolvent crystallization processes. *J Process Control*. 2008;18:856–864.
2. Lindenberg C, Krattli M, Cornel J, Mazzotti M, Brozio J. Design and optimization of a combined cooling/antisolvent process. *Cryst Growth Des*. 2009;9:1124–1136.
3. Widenski DJ, Abbas A, Romagnoli JA. A modeling approach for the non-isothermal antisolvent crystallization of a solute with weak temperature-dependent solubility. *Cryst Res Technol*. 2012;47 (5):491–504.
4. Woo XY, Nagy ZK, Tan RBH, Braatz RD. Adaptive concentration control of cooling and antisolvent crystallization with laser backscattering measurement. *Cryst Growth Des*. 2009;9(1):182–191.
5. Zhou GZ, Fujiwara M, Woo XY, Rusli E, Tung HH, Starbuck C, Davidson O, Ge Z, Braatz RD. Direct design of pharmaceutical antisolvent crystallization through concentration control. *Cryst Growth Des*. 2006;6:892–898.
6. Nowee SM, Abbas A, Romagnoli JA. Model-based optimal strategies for controlling particle size in antisolvent crystallization operations. *Cryst Growth Des*. 2008;8:2698–2706.
7. Nowee SM, Abbas A, Romagnoli JA. Antisolvent crystallization: Model identification, experimental validation and dynamic simulation. *Chem Eng Sci*. 2008;63:5457–5467.
8. Sheikhzadeh M, Trifkovic M, Rohani S. Real-time optimal control of an antisolvent isothermal semi-batch crystallization process. *Chem Eng Sci*. 2008;63:829–839.
9. Trifkovic M, Sheikhzadeh M, Rohani S. Kinetics estimation and single and multi-objective optimization of seeded, antisolvent, isothermal batch crystallizer. *Ind Eng Chem Res*. 2008;47:1586–1595.
10. Grosso M, Galàn O, Baratti R, Romagnoli JA. A Stochastic formulation for the description of the crystal size distribution in antisolvent crystallization processes. *AIChE J*. 2010;56(8):2077–2087.
11. Cogoni G, Grosso M, Baratti R, Romagnoli JA. Time evolution of the PSD in crystallization operations: An analytical solution based on Ornstein-Uhlenbeck process. *AIChE J*. 2012.doi:10.1002/aic.13760.
12. Tronci S, Grosso M, Baratti R, Romagnoli JA. A Stochastic approach for the prediction of psd in crystallization processes: analytical solution for the asymptotic behavior and parameter estimation. *Comput Chem Eng*. 2011;35(11):2318–2325.
13. Galan O, Grosso M, Baratti R, Romagnoli JA. Stochastic approach for the calculation of anti-solvent addition policies in crystallization operations: an application to a bench-scale semi-batch crystallizer. *Chem Eng Sci*. 2010;65:1797–1810.
14. Grosso M, Cogoni G, Baratti R, Romagnoli JA. Stochastic approach for the prediction of psd in crystallization processes: formulation and comparative assessment of different stochastic models. *Ind Eng Chem Res*. 2011;50:2133–2143.
15. Ramkrishna D. Population Balances. Theory and Applications to Particulate Systems in Engineering. San Diego: Academic Press; 2000.
16. Gelb A. Applied Optimal Estimator. Cambridge, MS: M.I.T. Press; 1988.

Manuscript received Sept. 28, 2012, and revision received Feb. 19, 2013.